Journal of Computational Physics 227 (2008) 9933–9954

Contents lists available at ScienceDirect

Journal of Computational Physics

journal homepage: www.elsevier.com/locate/jcp

A Schwarz generalized eigen-oscillation spectral element method (GeSEM) for 2-D high frequency electromagnetic scattering in dispersive inhomogeneous media

Wei Cai [a,*], Xia Ji [a], Jiguang Sun [b], Sihong Shao [c]

[a] Department of Mathematics and Statistics, University of North Carolina at Charlotte, Charlotte, NC 28223, United States
[b] Department of Applied Mathematics and Theoretical Physics, Delaware State University, Dover, DE 19901, United States
[c] School of Mathematical Sciences, Peking University, Beijing 100871, China

ARTICLE INFO

Article history:
Received 25 April 2008
Received in revised form 13 August 2008
Accepted 14 August 2008
Available online 29 August 2008

Keywords:
Eigen-oscillations
Spectral methods
Schwarz domain decomposition method
Radiation interface condition
Complex Helmholtz equations
High frequency scattering
Dispersive inhomogeneous media
Phase shift mask

ABSTRACT

In this paper, we propose a parallel Schwarz generalized eigen-oscillation spectral element method (GeSEM) for 2-D complex Helmholtz equations in high frequency wave scattering in dispersive inhomogeneous media. This method is based on the spectral expansion of complex generalized eigen-oscillations for the electromagnetic fields and the Schwarz non-overlapping domain decomposition iteration method. The GeSEM takes advantages of a special real orthogonality property of the complex eigen-oscillations and a new radiation interface condition for the system of equations for the spectral expansion coefficients. Numerical results validate the high resolution and the flexibility of the method for various materials.

1. Introduction

High frequency wave scattering in dispersive inhomogeneous media is one of the most challenging tasks facing the computational electromagnetics research communities. Several numerical methods have been used to simulate wave propagations in such inhomogeneous media, including the integral equation method [1], the finite difference time domain (FDTD) method [2], the finite element (FE) method [3], and the discontinuous Galerkin time domain (DGTD) method [4]. There are two related approximation issues in computing high frequency wave scattering in general media: (a) the approximation of inhomogeneity of the media and (b) the resolution of diffractions and interferences of high frequency waves in such media. Moreover, parallelization is a must-have for the numerical algorithms in realistic problems.

In this paper, a generalized eigen-oscillation spectral element method (GeSEM) is proposed where a Schwarz non-overlapping domain decomposition [5–8] is used to produce a highly parallel iterative algorithm for 2-D electromagnetic scattering problems. On the one hand, to handle the inhomogeneity of the media, piecewise polynomial approximations of the position dependent dielectric constant are used. On the other hand, to resolve high frequency waves, we employ a spectral method using complex generalized eigen-oscillations of non-self-adjoint complex Helmholtz operator along one

* Corresponding author. Tel.: +1 704 687 4581; fax: +1 704 687 6415/510 6415.
E-mail addresses: wcai@uncc.edu (W. Cai), xji3@uncc.edu (X. Ji), jsun@desu.edu (J. Sun), shaosihong@gmail.com (S. Shao).

0021-9991/$ - see front matter © 2008 Elsevier Inc. All rights reserved.
doi:10.1016/j.jcp.2008.08.012

of the coordinate directions. The reduced Helmholtz equations in the other direction are then solved with a Schwarz domain decomposition iterative scheme equipped with appropriate radiation interface conditions. The Schwarz domain decomposition methods for Helmholtz equations were studied in [5–8] where a radiation interface condition (Robin type) ensured the convergence of non-overlapping Schwarz iterations. Later, optimized radiation conditions were proposed, which realized higher order approximations of the radiation operator along the interface via tangential differential operators [9]. In the proposed GeSEM, we will extend the classical Enquist–Majda one way absorbing boundary condition [10] to a system of coupled equations for the spectral expansion coefficients in the reduced Helmholtz equations.

Traditionally, spectral methods based on eigenfunctions of singular Sturm–Liouville (S–L) operators have enjoyed many successes in the computational fluid dynamics and electromagnetics [11,12] due to the optimal resolution power of the Fourier expansions using such eigenfunctions. In general, either the Fourier exponentials or Chebyshev/Legendre orthogonal polynomials are used for the periodic or non-periodic problems, respectively. These basis functions form an orthogonal basis of a properly weighted L^2 space as a result of the Hermiticity of the S–L differential operators. However, there is a large class of problems, most importantly in the electromagnetic wave scattering in dispersive media such as metallic materials in phase shift mask of lithography for the VLSI process applications and soils in geophysical applications, where the dielectric constants are complex quantities. The relevant Helmholtz differential operators are no longer Hermitian, therefore, real eigenvalues and orthogonal eigenfunctions are not available for spectral representations of field solutions in such dispersive media. Nonetheless, there has been some work using the so-called generalized eigen-oscillations to study wave diffractions in dispersive media [13]. One of the unique properties of the complex generalized eigen-oscillations is a "real orthogonality" with a real inner-product between two complex functions. This real orthogonality allows the recovery of the expansion coefficients of a complex-valued function in terms of the generalized eigen-oscillations. Based on this property, we propose the GeSEM for scattering in dispersive media. It is important to note that the mathematical theory of the completeness, convergence and stability of the generalized eigen-oscillations is an ongoing research topic [14,15]. Thus, the focus of this paper is the construction of the numerical algorithm and its validation through tests to show the potential of the proposed method as a viable efficient method for scattering of high frequency waves in inhomogeneous dispersive media.

The computation of the eigenvalues and eigen-oscillations of complex Helmholtz equations is critical for a successful spectral method. The expansion of a function with these eigen-oscillations requires high degree of accuracy. Several numerical methods have been applied for computing complex Helmholtz eigenvalue problems such as multigrid methods [16] and high order nodal discontinuous Galerkin (DG) methods [17] for the multidimensional Maxwell eigenvalue problem. In [18], the authors discuss the issues of spurious eigenvalues of linear elliptic problems. In [19], it is shown that a wide class of stabilized DG methods can provide a spectrally correct approximation of the Laplace operator. In this paper, a stabilized DG method will be used to compute the eigenvalues and eigen-oscillations of complex Helmholtz operators.

One of the immediate applications of the proposed GeSEM is in the area of grating diffractions. A popular method for modeling grating structure, approximated by piecewise constant dielectric materials, is the Rigorous Coupled-Waveguide Analysis (RCWA), first proposed by Nyyssonen in [20] for the rigorous modeling of optical line-width measurement. Yuan applied this method to model light diffractions for 2D phase shift masks [21]. It is later extended to the modeling of 3D geometries mask [22]. In the RCWA, both the material properties and electromagnetic fields in each horizontal layer are expanded into Fourier series, algebraic equations for the expansion coefficients result from the Maxwell equations and the interface conditions between adjacent horizontal layers. Due to the use of Fourier series expansion, the RWCA is only applicable to periodic structures, thus edge effects in a grating will not be modeled correctly [23], and the method is not designed for parallel implementations. The RWCA may also have difficulties [24] when the number of grating elements become extremely large and the material is highly dissipative as in VLSI lithography masks due to the well-known Gibbs phenomena of Fourier expansion of discontinuous data [11]. The GeSEM is proposed to resolve these important issues, which will have impacts on the simulation of large scale mask in VLSI lithography processes (refer to [23] for a detailed comparison study regarding these issues between the RCWA and the GeSEM for modeling realistic alternating phase shift masks).

The rest of this paper is organized as follows. Section 2 describes the eigen-oscillation problem for complex Helmholtz equations with piecewise smooth complex coefficients. We also give a real orthogonality result of the generalized eigen-oscillations, important for spectral expansions of functions. Section 3 presents the GeSEM for scattering in 2-D inhomogeneous dispersive media. In Section 4, a Schwarz non-overlapping domain decomposition version of the GeSEM is proposed with appropriate radiation interface conditions. Section 5 discusses the high order approximation by DG methods for the eigen-oscillations and the eigenvalues. Numerical results in Section 6 demonstrate the fast convergence and high resolution power of the GeSEM for problems including those arising from phase shift mask where high frequency scattering through metal gratings is involved. Finally, a conclusion and discussion of the GeSEM are given in Section 7.

2. The generalized eigen-oscillations and real orthogonality

We consider the following generalized eigenvalue problem for a non-self-adjoint complex Helmholtz equation with homogeneous Dirichlet conditions at the end boundaries

$$\begin{cases} \frac{\mathrm{d}}{\mathrm{d}t}\left(p(t)\frac{\mathrm{d}u}{\mathrm{d}t}\right) + r(t)u = \lambda w(t)u \quad \text{for } t \in [-L, L], \\ u(-L) = u(L) = 0, \end{cases} \tag{1}$$

where $p(t)$, $r(t)$ and $w(t)$ are piecewise continuous complex functions. For electromagnetic scattering problems to be considered, we have

$$p(t) = w(t) = 1/\rho(t), \tag{2}$$

$$\text{where } \rho(t) = \begin{cases} \epsilon(t) - \text{Permittivity for transverse electric (TE) wave,} \\ \mu(t) - \text{Permeability for transverse magnetic (TM) wave.} \end{cases}$$

and

$$r(t) = \begin{cases} \omega^2\mu - \text{for transverse electric (TE) wave,} \\ \omega^2\epsilon - \text{for transverse magnetic (TM) wave.} \end{cases}$$

Assume that the interval $[-L,L]$ has been partitioned into the following mesh

$$-L = t_0 < t_1 < \cdots < t_N = L. \tag{3}$$

In each subinterval $I_i = (t_{i-1},t_i)$, $\rho(t)$ is a smooth function and u_i satisfies

$$\left(\frac{1}{\rho}u_i'\right)' + ru_i = \lambda\frac{1}{\rho}u_i, \quad \text{in } I_i, \quad \text{for } i = 1,\ldots,N, \tag{4}$$

and at each interior interface t_i, $i = 1,\ldots,N-1$, we impose the following transmission conditions:

$$u_i(t_i^-) = u_{i+1}(t_i^+), \tag{5}$$

$$\frac{1}{\rho_i^-}u_i'(t_i^-) = \frac{1}{\rho_i^+}u_i'(t_i^+), \tag{6}$$

where $\rho_i^\pm = \rho(t_i^\pm)$. And, at the end boundaries, homogeneous Dirichlet boundary conditions are given

$$u_1(t_0) = 0, \quad u_N(t_N) = 0. \tag{7}$$

The homogeneous boundary conditions in (7) arise from the use of perfect matched layer (PML) absorbing boundary conditions [25] for the computations of scattering waves (refer to Fig. 1 for the computational domain setup).

Multiplying (4) with a test function v_i and integrating by part, we obtain

$$-\int_{t_{i-1}}^{t_i}\frac{1}{\rho}u_i'v_i'\mathrm{d}s + \frac{1}{\rho}u_i'v_i|_{t_{i-1}}^{t_i} + \int_{t_{i-1}}^{t_i}ru_iv_i\mathrm{d}s = \lambda\int_{t_{i-1}}^{t_i}\frac{1}{\rho}u_iv_i\mathrm{d}s. \tag{8}$$

Summing (8) over all subintervals and applying the transmission conditions (5) and (6) and boundary conditions (7), we arrive at the following weak formulation for the eigenvalue problem: find $u \in H_0^1(-L,L)$ and $\lambda \in C$ such that

$$-\int_{-L}^{L}\frac{1}{\rho}u'v'\mathrm{d}s + \int_{-L}^{L}ruv\mathrm{d}s = \lambda\int_{-L}^{L}\frac{1}{\rho}uv\mathrm{d}s \tag{9}$$

for all $v \in H_0^1(-L,L)$.

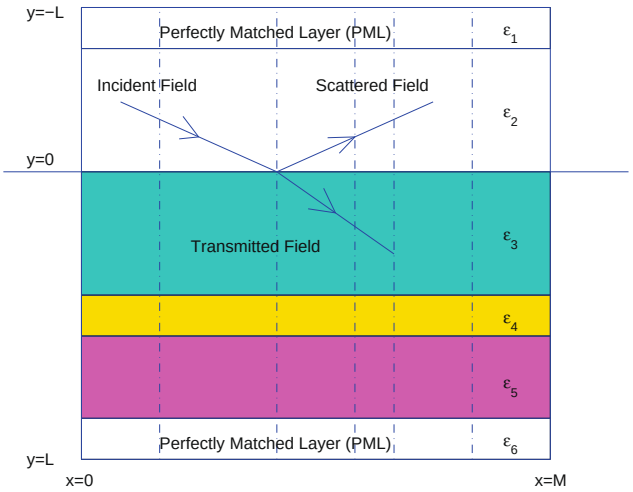

Fig. 1. Incident wave in a layered medium with PMLs on the top and at the bottom. Dashed vertical lines together with the horizontal lines form the domain decomposition for a multi-domain GeSEM with a different dielectric constant in each of the rectangular subdomains.

We present the following lemma on the orthogonality of the eigen-oscillations and its proof is straightforward, thus omitted.

Lemma 2.1 (Real orthogonality). *Suppose u_n and u_m are eigen-oscillations corresponding to two different eigenvalues λ_n and λ_m, then, u_n and u_m are orthogonal in the sense of*

$$\int_{-L}^{L} \frac{1}{\rho} u_n u_m ds = 0. \tag{10}$$

Remark 1. We would like to point out that the eigen-oscillations $\{u_n\}$ do not enjoy the Hermitian orthogonality, i.e.

$$\int_{-L}^{L} \frac{1}{\rho} u_m \overline{u_n} \mathrm{d}s \neq 0 \quad \text{for } n \neq m. \tag{11}$$

Assuming that the eigen-oscillations $\{u_n\}_{n=1}^{\infty}$ form a complete basis in $H_0^1(-L,L)$ and for all n, $\int_{-L}^{L} \frac{1}{\rho} u_n u_n \mathrm{d}s \neq 0$, we would like to estimate the decay rate of the coefficients of a function u which has been expressed in terms of the eigen-oscillations, i.e.

$$u = \sum_{n=1}^{\infty} A_n u_n \quad \text{and} \quad A_n = \frac{\int_{-L}^{L} \frac{1}{\rho} u u_n \mathrm{d}s}{\int_{-L}^{L} \frac{1}{\rho} u_n u_n \mathrm{d}s}. \tag{12}$$

It can be easily verified by using the differential equation (1) and an integration by part that

$$A_n = \mathrm{O}(\lambda_n^{-1}). \tag{13}$$

For self-adjoint problems, i.e. $\rho(t)$, $r(t)$ are real, the following asymptotic formula holds (see [26])

$$\lambda_n = \mathrm{O}(n^2), \quad \text{as } n \to \infty. \tag{14}$$

If the ρ is a small complex-perturbation of a real coefficient of a self-adjoint S–L problem, then Theorem 3.5.1 in [26] guarantees the eigenvalues of the complex S–L problem have the following asymptotic property:

$$|\lambda_n| = \mathrm{O}(n^2), \quad \text{as } n \to \infty. \tag{15}$$

3. Generalized eigen-oscillations spectral element method (GeSEM) for 2-D complex Helmholtz equations

Consider the following time harmonic Maxwell's equations:

$$\nabla \times \mathbf{H} = -\mathrm{i}\omega\epsilon\mathbf{E}, \tag{16}$$

$$\nabla \times \mathbf{E} = \mathrm{i}\omega\mu\mathbf{H}, \tag{17}$$

$$\nabla \cdot (\epsilon\mathbf{E}) = 0, \tag{18}$$

$$\nabla \cdot \mathbf{H} = 0. \tag{19}$$

By eliminating either **E** or **H** from Eqs. (16) and (17), we have a vector Helmholtz equation for **H**

$$-\nabla \times \left(\frac{1}{\epsilon}\nabla \times \mathbf{H}\right) + \omega^2\mu\mathbf{H} = 0, \tag{20}$$

or for **E**

$$-\nabla \times \left(\frac{1}{\mu}\nabla \times \mathbf{E}\right) + \omega^2\epsilon\mathbf{E} = 0. \tag{21}$$

For a TE-polarized wave, the magnetic field has only a z-component, i.e., $\mathbf{H} = (0,0,H_z)$, resulting in a scalar Helmholtz equation for H_z

$$\frac{\partial}{\partial x}\left(\frac{1}{\epsilon}\frac{\partial H_z}{\partial x}\right) + \frac{\partial}{\partial y}\left(\frac{1}{\epsilon}\frac{\partial H_z}{\partial y}\right) + \omega^2\mu H_z = 0, \tag{22}$$

with the following interface conditions:

$$[H_z] = 0, \left[\frac{1}{\epsilon}\frac{\partial H_z}{\partial n}\right] = 0, \tag{23}$$

where $[\cdot]$ denotes the jump and $\frac{\partial}{\partial n}$ is the normal derivative at a material interface.

Similarly, for a TM-polarized wave, the electric field has only a z-component, i.e., $\mathbf{E} = (0,0,E_z)$, which again satisfies a scalar Helmholtz equation

$$\frac{\partial}{\partial x}\left(\frac{1}{\mu}\frac{\partial E_z}{\partial x}\right) + \frac{\partial}{\partial y}\left(\frac{1}{\mu}\frac{\partial E_z}{\partial y}\right) + \omega^2\epsilon E_z = 0, \tag{24}$$

with the interface conditions

$$[E_z] = 0, \quad \left[\frac{1}{\mu}\frac{\partial E_z}{\partial n}\right] = 0. \tag{25}$$

3.1. Single domain case – a layered media

Consider a layered media with an incident plane wave impinging from above and piecewise constant ϵ (see Fig. 1). The top and bottom of the computational domain are terminated by two layers of PML regions defined in Section 6.1.

The total field H_z can be decomposed into the incident field and the scattering field

$$\begin{cases} H_z(x,y) = H_z^i(x,y) + H_z^s(x,y), & y > 0, \\ H_z(x,y) = H_z^s(x,y), & y < 0, \end{cases} \tag{26}$$

and satisfies the following transmission conditions on material interfaces:

$$\begin{cases} H_z(x,y_i^-) = H_z(x,y_i^+), \\ \frac{1}{\epsilon(y_i^-)}\frac{\partial H_z(x,y_i^-)}{\partial y} = \frac{1}{\epsilon(y_i^+)}\frac{\partial H_z(x,y_i^+)}{\partial y}, \end{cases} \tag{27}$$

where y_i is the interface between layer i and $i+1$. From the continuity of H_z across the horizontal material interfaces, we obtain the transmission conditions for the scattering waves at $y_i \neq 0$

$$\begin{cases} H_z^s(x,0^-) = H_z^s(x,0^+), \\ \frac{1}{\epsilon(y_i^-)}\frac{\partial H_z^s(x,y_i^-)}{\partial y} = \frac{1}{\epsilon(y_i^+)}\frac{\partial H_z^s(x,y_i^+)}{\partial y}. \end{cases} \tag{28}$$

On the interface $y_i = 0$, we have

$$\begin{cases} H_z^s(x,0^-) - H_z^s(x,0^+) = H_z^i(x,0^+), \\ \frac{1}{\epsilon(0^-)}\frac{\partial H_z^s}{\partial y}(x,0^-) - \frac{1}{\epsilon(0^+)}\frac{\partial H_z^s}{\partial y}(x,0^+) = \frac{1}{\epsilon(0^+)}\frac{\partial H_z^i}{\partial y}(x,0^+). \end{cases} \tag{29}$$

Moreover, at the outer boundaries of the PML regions in Fig. 1, homogeneous Dirichlet boundary conditions are imposed for the scattering waves, namely,

$$H_z^s(x,\pm L) = 0. \tag{30}$$

Now, let $\{\phi_p(y)\}$ be the eigen-oscillations of the generalized eigenvalue problem of (1) with $\rho = \epsilon$ and suitable PML absorbing boundary conditions at the ends. Consider the following series expansion of the scattering wave:

$$H_z^s(x,y) = \alpha(x)\xi_1(y) + \beta(x)\xi_2(y) + \sum_{p=1}^{\infty} c_p(x)\phi_p(y). \tag{31}$$

The first two terms in (31) will be chosen to account for the inhomogeneous interface conditions (29) at $y = 0$ while the series expansion will satisfy the homogeneous interface conditions at all $y = y_i$. Meanwhile, both of them will satisfy the Helmholtz equation (22).

Plugging the expansion in (31) into the Helmholtz equation (22) and using (1), we have

$$\sum_{p=1}^{\infty}\left[\lambda_p c_p(x) + c_p''(x)\right]\frac{1}{\epsilon(y)}\phi_p(y) = 0.$$

From the real orthogonality condition (10), we can see that $c_p(x)$ satisfies

$$c_p''(x) + \lambda_p c_p(x) = 0, \tag{32}$$

whose general solution is given by

$$c_p(x) = A_p \exp(-\mathrm{i}\sqrt{\lambda_p}x) + B_p \exp(\mathrm{i}\sqrt{\lambda_p}x). \tag{33}$$

Next, to derive the expression of $\alpha(x)\xi_1(y) + \beta(x)\xi_2(y)$, we consider the function

$$D_1(x,y) = \alpha(x)\xi_1(y), \tag{34}$$

where

$$\alpha(x) = H_z^i(x,0^-). \tag{35}$$

If the incident wave is a plane wave given by

$$H_z^i = H_0 \exp(-\mathrm{i}k_x x - \mathrm{i}k_y y), \tag{36}$$

we have

$$\alpha''(x) = \frac{\partial^2}{\partial x^2} H_z^i(x,0) = -k_x^2 H_z^i(x,0), \tag{37}$$

then

$$\alpha''(x) = -k_x^2 \alpha(x). \tag{38}$$

Plugging (34) into (22), we have

$$\alpha(x)\left(\frac{1}{\epsilon(y)}\xi_1'(y)\right)' + \frac{1}{\epsilon(y)}\alpha''(x)\xi_1(y) + \omega^2\mu\alpha(x)\xi_1(y) = 0.$$

Using (38), we obtain

$$\alpha(x)\left[\left(\frac{1}{\epsilon(y)}\xi_1'(y)\right)' + \omega^2\mu\xi_1(y) - \frac{k_x^2}{\epsilon(y)}\xi_1(y)\right] = 0.$$

Hence, we can see that $\xi_1(y)$ can be selected as the solution of the following problem to account for the inhomogeneous jump conditions for the function at $y = 0$:

$$\begin{cases} \left(\frac{1}{\epsilon(y)}\xi_1'(y)\right)' + [\omega^2\mu - \frac{k_x^2}{\epsilon(y)}]\xi_1(y) = 0, \\ \xi_1(\pm L) = 0, \\ \xi_1(0^-) - \xi_1(0^+) = 1, \\ \frac{1}{\epsilon(0^-)}\xi_1'(0^-) - \frac{1}{\epsilon(0^+)}\xi_1'(0^+) = 0. \end{cases} \tag{39}$$

Similarly, we set the function

$$D_2(x,y) = \beta(x)\xi_2(y), \tag{40}$$

where

$$\beta(x) = \frac{\partial}{\partial y} H_z^i(x,0^+). \tag{41}$$

And $\xi_2(y)$ can be defined to account for the inhomogeneous jump conditions for the derivative of the function value at $y = 0$

$$\begin{cases} \left(\frac{1}{\epsilon(y)}\xi_2'(y)\right)' + [\omega^2\mu - \frac{k_x^2}{\epsilon(y)}]\xi_2(y) = 0, \\ \xi_2(\pm L) = 0, \\ \xi_2(0^-) - \xi_2(0^+) = 0, \\ \frac{1}{\epsilon(0^-)}\xi_2'(0^-) - \frac{1}{\epsilon(0^+)}\xi_2'(0^+) = \frac{1}{\epsilon(0^+)}. \end{cases} \tag{42}$$

Finally, we can easily verify that

$$H_z^s(x,y) = \alpha(x)\xi_1(y) + \beta(x)\xi_2(y) + \sum_{p=1}^{\infty} c_p(x)\phi_p(y), \tag{43}$$

solves Eq. (22) with interface conditions (23) for an incident plane wave given by (36).

Similar formulation can be done for the E_z component for TM-polarized waves.

3.2. Multi-domain case - general inhomogeneous media

We consider the scattering of an incident plane wave in an inhomogeneous media where the dielectric constant is approximated by piecewise constants or linear polynomials over each rectangular subdomain $\Omega_{i,j}$ (formed by horizontal solid lines and vertical dashed lines in Fig. 1), i.e.

$$\epsilon_{ij}(x,y) = \epsilon_{ij}^x + \epsilon_{ij}^y, \quad (x,y) \in \Omega_{i,j}, \tag{44}$$

where ϵ_{ij}^x and ϵ_{ij}^y are constants (TE wave) or linear functions (TM wave) of x and y, respectively. By selecting the size of $\Omega_{i,j}$, we can approximate general inhomogeneous media within any given accuracy.

3.2.1. TE wave

For the TE case, in each vertical strip region, $\Omega_i = \cup_j \Omega_{i,j} = \{(x,y)|, x_{i-1} \leqslant x \leqslant x_i\}$, $\epsilon_{ij}(x,y)$ is assumed to be constant in each subdomain $\Omega_{i,j}$ and we can set $\epsilon_{ij}^x = 0$, and $\epsilon_{ij}^y = \epsilon_{ij}(x,y)$. Now $H_z^s(x,y)$ can be written as

$$H_z^s(x,y) = \alpha^i(x)\xi_1^i(y) + \beta^i(x)\xi_2^i(y) + \sum_{p=1}^{\infty} c_p^i(x)\phi_p^i(y), \tag{45}$$

where $\phi_p^i(y)$ is the eigen-oscillation satisfying

$$\left(\frac{1}{\epsilon_{i,*}^y}(\phi_p^i(y))'\right)' + \omega^2\mu\phi_p^i(y) = \lambda_p^i\frac{1}{\epsilon_{i,*}^y}\phi_p^i(y), \tag{46}$$

and $\xi_1^i(y)$ and $\xi_2^i(y)$ are determined by Eqs. (39) and (42).

Plugging the expansion (45) into (22), we can get

$$\sum_{p=1}^{\infty}\left[c_p^i(x)\left(\frac{1}{\epsilon_{i,*}^y}(\phi_p^i(y))'\right)' + \frac{1}{\epsilon_{i,*}^y}(c_p^i(x))''\phi_p^i(y)\right] + \omega^2\sum_{p=1}^{\infty}c_p(x)\phi_p^i(y) = 0,$$

which yields

$$\sum_{p=1}^{\infty}\left[\frac{d^2}{dx^2}c_p^i(x) + \lambda_p c_p^i(x)\right]\frac{1}{\epsilon_{i,j}^y}\phi_p(y) = 0. \tag{47}$$

Using the real orthogonality of the eigen-oscillations (10), we get

$$\frac{d^2}{dx^2}c_q^i + \lambda_q c_q^i = 0. \tag{48}$$

Rewriting the above equations into a vector form, we have

$$\frac{d^2}{dx^2}C^i + \Lambda^i C^i = 0, \tag{49}$$

where $C^i = (c_1^i, \ldots, c_N^i)^T$, and Λ^i is defined by

$$\Lambda_{pq}^i = \lambda_q\delta_{pq}, \tag{50}$$

and is a complex diagonal matrix. Here δ_{pq} is the Kronecker delta function. Eq. (49) will be solved analytically or by a Chebyshev collocation method especially in the TM wave case below when Λ^i is not a diagonal matrix anymore and becomes a function of x.

3.2.2. TM wave

For the TM case, the Helmholtz equation (22) for the E_z component can be rewritten as

$$\frac{\partial}{\partial x}\left(\frac{1}{\mu}\frac{\partial E_z}{\partial x}\right) + \frac{\partial}{\partial y}\left(\frac{1}{\mu}\frac{\partial E_z}{\partial y}\right) + \omega^2(\epsilon_{ij}^x + \epsilon_{ij}^y)E_z = 0, \quad (x,y) \in \Omega_{i,j} \tag{51}$$

where ϵ_{ij}^x and ϵ_{ij}^y in principle can be any function of x and y (taken to be linear though in this paper), respectively.

In each vertical strip region, $\Omega_i = \cup_j\Omega_{i,j} = \{(x,y)|, x_{i-1} \leqslant x \leqslant x_i\}$, $E_z^s(x,y)$ can be written as

$$E_z^s(x,y) = \alpha^i(x)\xi_1^i(y) + \beta^i(x)\xi_2^i(y) + \sum_{p=1}^{\infty}c_p^i(x)\phi_p^i(y). \tag{52}$$

Here $\phi_p^i(y)$ is the eigen-oscillation satisfying

$$\left(\frac{1}{\mu}(\phi_p^i(y))'\right)' + \omega^2\epsilon_{ij}^y\phi_p^i(y) = \lambda_p^i\frac{1}{\mu}\phi_p^i(y). \tag{53}$$

And $\xi_1^i(y)$ and $\xi_2^i(y)$ satisfy Eqs. (39) and (42) with all ϵ and μ exchanged for each strip Ω_i.

Again, using the real orthogonality of the eigen-oscillations (10), we get

$$\frac{d^2}{dx^2}c_q^i(x) + \lambda_q c_q^i + \Sigma_p\kappa_{pq}^i c_p^i = 0. \tag{54}$$

where

$$\kappa_{pq}^i = \kappa_{pq}^i(x) = \omega^2\int_{-L}^{L}\frac{\epsilon_{ij}^x}{\mu}\phi_p^i(y)\phi_q^i(y)dy, \tag{55}$$

which results in the same form of equations for the coefficient C^i as in (49), and here Λ^i defined by $\Lambda_{pq}^i = \lambda_q\delta_{pq} + \kappa_{pq}^i$ will be a complex symmetric matrix which can not be diagonalized in general and $\Lambda^i = \Lambda^i(x)$ is a function of x within each subdomain Ω_i.

4. Parallel Schwarz GeSEM

In this section, we will apply a non-overlapping Schwarz domain decomposition method to implement the multi-domain GeSEM proposed in the previous section with appropriate radiation interface conditions for the coupled 1-D systems for the expansion coefficients C in (49).

4.1. Radiation conditions

Since in general the matrix Λ can not be diagonalized, the traditional Enqusit–Majda's one-way wave condition [10] for the scalar case does not apply. Here, we will propose a more general radiation condition for the case of non-diagonalizable matrix Λ.

4.1.1. A simple case – 2×2 Jordan block

Suppose after a similarity transformation by a complex matrix U, Λ becomes a 2×2 Jordan block, i.e.

$$U\Lambda U^{-1} = \begin{bmatrix} \lambda & 1 \\ 0 & \lambda \end{bmatrix} = \begin{bmatrix} k^2 & 1 \\ 0 & k^2 \end{bmatrix}. \tag{56}$$

Defining $D = UC = \begin{bmatrix} d_1 \\ d_2 \end{bmatrix}$ and assuming constant U near the boundary points, the new variable D satisfies

$$\begin{bmatrix} d_1 \\ d_2 \end{bmatrix}'' + \begin{bmatrix} k^2 & 1 \\ 0 & k^2 \end{bmatrix} \begin{bmatrix} d_1 \\ d_2 \end{bmatrix} = 0. \tag{57}$$

The second variable d_2 satisfies

$$d_2'' + k^2 d_2 = 0, \tag{58}$$

whose general solution can be written as

$$d_2(x) = c_1 \exp(\mathrm{i}kx) + c_2 \exp(-\mathrm{i}kx). \tag{59}$$

In an interval $[a,b]$, the radiation condition for $d_2(x)$ at $x = b$ is

$$\left(\frac{\mathrm{d}}{\mathrm{d}x} + \mathrm{i}k\right) d_2|_{x=b} = 0, \tag{60}$$

which is the same as the traditional one-way radiation condition.

To find the radiation condition for $d_1(x)$ which satisfies

$$d_1'' + k^2 d_1 = -d_2, \tag{61}$$

where d_2 acts as a resonant forcing term, we write the general solution for d_1 as

$$d_1(x) = (e_1 x + f_1) \exp(\mathrm{i}kx) + (e_2 x + f_2) \exp(-\mathrm{i}kx). \tag{62}$$

Term $(e_2x + f_2)\exp(-\mathrm{i}kx)$ then satisfies

$$[\exp(\mathrm{i}kx) d_1(x)]'' = (e_2 x + f_2)'' = 0, \tag{63}$$

so

$$[d_1'' + 2(\mathrm{i}k) d_1' + (\mathrm{i}k)^2 d_1]|_{x=b} = 0. \tag{64}$$

Using (61), we can get

$$2\mathrm{i}k d_1' - 2k^2 d_1 - d_2 = 0, \tag{65}$$

which is the radiation condition for d_1 at $x = b$.

4.1.2. General case – $n \times n$ Jordan block

In fact, we can rewrite the radiation condition for the above simple case as

$$\frac{\mathrm{d}}{\mathrm{d}x} \begin{bmatrix} d_1 \\ d_2 \end{bmatrix} + \mathrm{i}K \begin{bmatrix} d_1 \\ d_2 \end{bmatrix} = 0, \tag{66}$$

where

$$K = \begin{bmatrix} k & \frac{1}{2k} \\ 0 & k \end{bmatrix}. \tag{67}$$

It is easy to check that

$$K^2 = \Lambda,$$

thus, K is simply the square root of Λ

$$K = \sqrt{\Lambda}. \tag{68}$$

Therefore, in the case of a $n \times n$ Jordan block $U\Lambda U^{-1} = k^2 I + \Gamma$, where

$$\Gamma = \begin{bmatrix} 0 & 1 & 0 & \cdots & 0 \\ 0 & 0 & 1 & \cdots & 0 \\ \vdots & \vdots & \ddots & \ddots & \vdots \\ 0 & 0 & \cdots & 0 & 1 \\ 0 & 0 & \cdots & 0 & 0 \end{bmatrix}_{n\times n}, \tag{69}$$

from mathematical induction, we can show that

$$K = \sqrt{k^2 I + \Gamma} = k\left(I + \frac{1}{k^2}\Gamma\right)^{\frac{1}{2}} = k\sum_{l=0}^{n-1} \frac{f^{(l)}(0)}{l!}\frac{1}{k^{2l}}\Gamma^l, \tag{70}$$

where

$$f(x) = \sqrt{1+x}. \tag{71}$$

Therefore, the radiation boundary condition is

$$\frac{\mathrm{d}}{\mathrm{d}x}\begin{bmatrix} d_1 \\ \vdots \\ d_n \end{bmatrix} + \mathrm{i}K\begin{bmatrix} d_1 \\ \vdots \\ d_n \end{bmatrix} = 0, \tag{72}$$

which reads in term of the original variable

$$\frac{\mathrm{d}}{\mathrm{d}x}C + \mathrm{i}KC = 0. \tag{73}$$

4.2. Schwarz GeSEM

Using the complex generalized eigen-oscillations along y direction, the Helmholtz equations (22) or (24) are reduced to a system of 1-D Helmholtz equations (49) in x-direction. A Schwarz domain decomposition iterative scheme will be used to solve (49) with the radiation interface conditions. Fig. 2 is the sketch for the Schwarz iteration, in order to compute the solution in subdomain $I_j = [x_{j-1}, x_j]$ for the iteration step n, the information on the neighboring domain I_{j-1} and I_{j+1} at the previous step $n-1$ is used to provide the boundary condition at x_{j-1}, x_j by a Robin boundary condition using the radiation operator in (73).

4.2.1. TM wave

The solutions for the scattering wave $E^s_{z,j}$ in different strips are connected by interface condition (25) via the radiation operator (73) with the eigen-oscillation expansion for the $E^s_{z,j}$ in (52) for adjacent strips and the real orthogonality property (10) of the eigen-oscillations, namely

$$\begin{cases} c_q^j = g_j \equiv \int_{-L}^{L}(\alpha^{j+1}\xi_1^{j+1} + \beta^{j+1}\xi_2^{j+1} + \Sigma c_p^{j+1}\phi_p^{j+1})\phi_q^j \mathrm{d}y - \int_{-L}^{L}(\alpha^j\xi_1^j + \beta^j\xi_2^j)\phi_q^j \mathrm{d}y, \\ \frac{\mathrm{d}c_q^j}{\mathrm{d}x} = f_j \equiv \int_{-L}^{L}\left(\frac{\mathrm{d}\alpha^{j+1}}{\mathrm{d}x}\xi_1^{j+1} + \frac{\mathrm{d}\beta^{j+1}}{\mathrm{d}x}\xi_2^{j+1} + \Sigma\frac{\mathrm{d}c_q^{j+1}}{\mathrm{d}x}\phi_p^{j+1}\right)\phi_q^j \mathrm{d}y - \int_{-L}^{L}\left(\frac{\mathrm{d}\alpha^j}{\mathrm{d}x}\xi_1^j + \frac{\mathrm{d}\beta^j}{\mathrm{d}x}\xi_2^j\right)\phi_q^j \mathrm{d}y, \end{cases} \tag{74}$$

which can be combined into the radiation operator (73) to give the following radiation interface condition for the GeSEM at the right end boundary of the subdomain I_j

$$\frac{\mathrm{d}C^j}{\mathrm{d}x} + \mathrm{i}K(x_j^-)C^j = F + \mathrm{i}K(x_j^-)G, \tag{75}$$

where $C^j = \{c_1^j, c_2^j, c_3^j, \ldots\}$, $F = F(C^{j+1}, \alpha^{j+1}, \beta^{j+1}, \xi_1^{j+1}, \xi_2^{j+1}) \equiv \{f_j\}$ and $G = G(C^{j+1}, \alpha, \beta, \xi_1, \xi_2) \equiv \{g_j\}$.

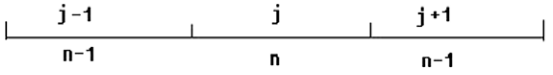

Fig. 2. Schwarz iteration in x-direction.

A similar radiation interface condition at the left end boundary of subdomain I_{j+1} can be obtained

$$\frac{\mathrm{d}C^{j+1}}{\mathrm{d}x} - iK(x_j^+)C^{j+1} = F - iK(x_j^+)G, \tag{76}$$

where $F = F(C^j, \alpha^j, \beta^j, \xi_1^j, \xi_2^j) \equiv \{f_j\}, G = G(C^j, \alpha, \beta, \xi_1, \xi_2) \equiv \{g_j\}$, and

$$\begin{cases} g_j = \int_{-L}^{L} (\alpha^j \xi_1^j + \beta^j \xi_2^j + \Sigma c_p^j \phi_p^j)\phi_q^{j+1}\mathrm{d}y - \int_{-L}^{L} (\alpha^{j+1}\xi_1^{j+1} + \beta^{j+1}\xi_2^{j+1})\phi_q^{j+1}\mathrm{d}y, \\ f_j = \int_{-L}^{L} \left(\frac{\mathrm{d}\alpha^j}{\mathrm{d}x}\xi_1^j + \frac{\mathrm{d}\beta^j}{\mathrm{d}x}\xi_2^j + \Sigma \frac{\mathrm{d}c_q^j}{\mathrm{d}x}\phi_p^j\right)\phi_q^{j+1}\mathrm{d}y - \int_{-L}^{L} \left(\frac{\mathrm{d}\alpha^{j+1}}{\mathrm{d}x}\xi_1^{j+1} + \frac{\mathrm{d}\beta^{j+1}}{\mathrm{d}x}\xi_2^{j+1}\right)\phi_q^{j+1}\mathrm{d}y. \end{cases} \tag{77}$$

Finally, for the end boundaries, we simply have an homogeneous radiation condition

$$\frac{\mathrm{d}C^j}{\mathrm{d}x} \pm \mathrm{i}KC^j = \mathbf{0}, \tag{78}$$

where K is evaluated inside the computational domain and +/− sign is for the right/left boundary of the computational domain, respectively.

4.2.2. TE wave

Similar procedure can be done for the TE wave, the solution for the scattering wave $H_{z,j}^s$ in different strips is connected by interface condition (23) via the radiation operator (73). Using the expansion for the $H_{z,j}^s$ in (31) for adjacent strips and again the real orthogonality property (10) of the eigen-oscillations, we have

$$\begin{cases} c_q^j = g \equiv \int_{-L}^{L} \frac{1}{\varepsilon_{j,*}^y}(\alpha^{j+1}\xi_1^{j+1} + \beta^{j+1}\xi_2^{j+1} + \Sigma c_p^{j+1}\phi_p^{j+1})\phi_q^j\mathrm{d}y - \int_{-L}^{L} \frac{1}{\varepsilon_{j,*}^y}(\alpha^j\xi_1^j + \beta^j\xi_2^j)\phi_q^j\mathrm{d}y, \\ \frac{\mathrm{d}c_q^j}{\mathrm{d}x} = f \equiv \int_{-L}^{L} \frac{1}{\varepsilon_{j+1,*}^y}\left(\frac{\mathrm{d}\alpha^{j+1}}{\mathrm{d}x}\xi_1^{j+1} + \frac{\mathrm{d}\beta^{j+1}}{\mathrm{d}x}\xi_2^{j+1} + \Sigma \frac{\mathrm{d}c_q^{j+1}}{\mathrm{d}x}\phi_p^{j+1}\right)\phi_q^j\mathrm{d}y - \int_{-L}^{L} \frac{1}{\varepsilon_{j,*}^y}\left(\frac{\mathrm{d}\alpha^j}{\mathrm{d}x}\xi_1^j + \frac{\mathrm{d}\beta^j}{\mathrm{d}x}\xi_2^j\right)\phi_q^j\mathrm{d}y, \end{cases} \tag{79}$$

which can be combined into the radiation operator (73) for the following radiation interface condition for the GeSEM at the right end boundary of the subdomain I_j

$$\frac{\mathrm{d}C^j}{\mathrm{d}x} + \mathrm{i}K(x_j^-)C^j = F + iK(x_j^-)G, \tag{80}$$

where $C^j = \{c_1^j, c_2^j, c_3^j, \ldots\}, F = F(C^{j+1}, \alpha^{j+1}, \beta^{j+1}, \xi_1^{j+1}, \xi_2^{j+1}) \equiv \{f_j\}$ and

$G = G(C^{j+1}, \alpha^{j+1}, \beta^{j+1}, \xi_1^{j+1}, \xi_2^{j+1}) = \{g_j\}$.

A similar radiation interface condition at the left end boundary of subdomain I_{j+1} can be obtained

$$\frac{\mathrm{d}C^{j+1}}{\mathrm{d}x} - \mathrm{i}K(x_j^+)C^{j+1} = F - iK(x_j^+)G, \tag{81}$$

where $F = F(C^j, \alpha^j, \beta^j, \xi_1^j, \xi_2^j) \equiv \{f_j\}, G = G(C^j, \alpha^j, \beta^j, \xi_1^j, \xi_2^j) \equiv \{g_j\}$,

$$\begin{cases} g_j = \int_{-L}^{L} \frac{1}{\varepsilon_{*,j+1}^y}(\alpha^j\xi_1^j + \beta^j\xi_2^j + \Sigma c_p^j\phi_p^j)\phi_q^{j+1}\mathrm{d}y - \int_{-L}^{L} \frac{1}{\varepsilon_{*,j+1}^y}(\alpha^{j+1}\xi_1^{j+1} + \beta^{j+1}\xi_2^{j+1})\phi_q^{j+1}\mathrm{d}y, \\ f_j = \int_{-L}^{L} \frac{1}{\varepsilon_{*,j}^y}\left(\frac{\mathrm{d}\alpha^j}{\mathrm{d}x}\xi_1^j + \frac{\mathrm{d}\beta^j}{\mathrm{d}x}\xi_2^j + \Sigma \frac{\mathrm{d}c_q^j}{\mathrm{d}x}\phi_p^j\right)\phi_q^{j+1}\mathrm{d}y - \int_{-L}^{L} \frac{1}{\varepsilon_{*,j}^y}\left(\frac{\mathrm{d}\alpha^{j+1}}{\mathrm{d}x}\xi_1^{j+1} + \frac{\mathrm{d}\beta^{j+1}}{\mathrm{d}x}\xi_2^{j+1}\right)\phi_q^{j+1}\mathrm{d}y. \end{cases} \tag{82}$$

Finally, for the end boundaries, we simply have an homogeneous radiation condition

$$\frac{\mathrm{d}C^j}{\mathrm{d}x} \pm iKC^j = \mathbf{0}. \tag{83}$$

It is clear that the solution at the current time step in I_j only depends on the solution at previous step in neighboring subdomains, as a result, this algorithm is highly parallel.

Remark 2. The convergence of the proposed Schwarz GeSEM depends strongly on the magnitude of the imaginary parts of the eigenvalues in K as shown in Appendix for the case of two subdomains.

5. Numerical issues of eigen-oscillations and eigenvalues

5.1. Computations of eigen-oscillations by DG Methods

In this section, we apply the DG method for the generalized eigenvalue problem. For illustration purpose, we set $r(t) = 1$ in (1). Following [27], we introduce

$$q = u'(t),$$

and obtain a first-order system

$$\frac{\mathrm{d}}{\mathrm{d}x}\left(\frac{1}{\rho(t)}q(t)\right) + u = \lambda\frac{1}{\rho(t)}u, \tag{84}$$

$$u'(t) - q(t) = 0. \tag{85}$$

Discretize $[-L,L]$ into N elements uniformly and let $I_j = [t_{j-1},t_j]$. For simplicity, the interfaces of the material layers coincide with the interfaces of mesh grids and we define the finite element space as

$$V_h = \{v \in L^2(-L,L) : v|_{I_j} \in P^k(I_j), \quad j = 1,\ldots,N\},$$

where P^k denotes the space of polynomials on I_j of degree at most k. The discrete eigenvalue problem is then to find (λ, u_h, q_h) such that

$$-\int_{I_j}\frac{1}{\rho}q_h\frac{\mathrm{d}v_{h,u}}{\mathrm{d}t}\mathrm{d}s + h_{q,j+1/2}v_{h,u}(t_{j+1}^-) - h_{q,j}v_{h,u}(t_j^+) + \int_{I_j}u_h v_{h,u}\mathrm{d}s = \lambda\int_{I_j}\frac{1}{\rho}u_h v_{h,u}\mathrm{d}x \quad \forall v_{h,u} \in P^k(I_j) \tag{86}$$

$$-\int_{I_j}u_h\frac{\mathrm{d}v_{h,q}}{\mathrm{d}t}\mathrm{d}s + h_{u,j+1/2}v_{h,q}(t_{j+1/2}^-) - h_{u,j-1/2}v_{h,q}(t_{j-1/2}^+) = \int_{I_j}q_h v_{h,q}\mathrm{d}s \quad \forall v_{h,q} \in P^k(I_j), \tag{87}$$

where $(h_{q,j}, h_{u,j})$ is the numerical flux defined by

$$h_{u,j} = \{u_j\}, \tag{88}$$

$$h_{q,j} = \{\frac{1}{\rho_j}q_j\} - S_h([u_j]), \tag{89}$$

when t_j is an interior node and

$$h_{u,0} = 0, \tag{90}$$

$$h_{q,j} = \frac{1}{\rho_j}q_j - S_h(u_j), \tag{91}$$

when t_j is a boundary node. Here, we used the notations

$$[w_j] = w_j^+ - w_j^-, \quad \{w_j\} = (w_j^+ + w_j^-)/2,$$

across a mesh point t_j.

Remark 3. The stabilization function $S_h(\cdot)$ is defined as $S_h(\phi) = \alpha h^{-1}$ with $\alpha > 0$ independent of the mesh size. Note that this choice of numerical flux leads to a stable DG method. For other choices of numerical flux and the general discussion of stability issues, we refer to [28].

For $t \in I_j$, let

$$u_h(t) = \sum_{k=1}^{s}u_k^j\phi_k^j(t), \tag{92}$$

$$q_h(t) = \sum_{k=1}^{s}q_k^j\phi_k^j(t), \tag{93}$$

where s is the total number of the basis functions and ϕ_k are basis functions.

On each interval I_j, same order of Legendre polynomials will be used as the basis functions for $P^k(I_j)$ given by

$$\phi_k^j(t) = L_k(\xi(t)), \quad k = 1,2,\ldots,s, \quad t \in I_j,$$

$$\xi^j(t) = \frac{2(t-t_{j-1})}{h_j},$$

where h_j is the length of the jth interval and L_k is the Legendre polynomial of degree $k-1$.

Using the definition of the numerical flux and replacing u_h and q_h defined above, we obtain from (86) and (87)

$$-S_\rho^j\mathbf{q}^j + \frac{1}{2}\Phi_r\left(\frac{1}{\rho(t_{j+1}^-)}\Phi_r^{\mathrm{T}}\mathbf{q}^j + \frac{1}{\rho(t_{j+1}^+)}\Phi_l^{\mathrm{T}}\mathbf{q}^{j+1}\right) - \frac{1}{2}\Phi_l\left(\frac{1}{\rho(t_j^-)}\Phi_r^{\mathrm{T}}\mathbf{q}^{j-1} + \frac{1}{\rho(t_j^+)}\Phi_l^{\mathrm{T}}\mathbf{q}^j\right)$$
$$-\Phi_r(\Phi_l^{\mathrm{T}}\mathbf{u}^{j+1} - \Phi_l^{\mathrm{T}}\mathbf{u}^j) + \Phi_l(\Phi_l^{\mathrm{T}}\mathbf{u}^j - \Phi_l^{\mathrm{T}}\mathbf{u}^{j-1}) + M^j\mathbf{u}^j = \lambda M_\rho^j\mathbf{u}^j,$$

$$-S^j\mathbf{u}^j + \frac{1}{2}\Phi_r(\Phi_r^{\mathrm{T}}\mathbf{u}^j + \Phi_l^{\mathrm{T}}\mathbf{u}^{j+1}) - \frac{1}{2}\Phi_l(\Phi_r^{\mathrm{T}}\mathbf{u}^{j-1} + \Phi_l^{\mathrm{T}}\mathbf{u}^j) = M^j\mathbf{q}^j,$$

where S and S^ρ are the local stiffness matrices given by

$$S^j_{nm} = \int_{I_j} \phi_m \frac{\mathrm{d}\phi_n}{\mathrm{d}t}\mathrm{d}s,$$
$$S^j_{\rho,nm} = \int_{I_j} \frac{1}{\rho}\phi_m \frac{\mathrm{d}\phi_n}{\mathrm{d}t}\mathrm{d}s,$$

M^j and M^j_ρ are the local mass matrices given by

$$M^j_{nm} = \int_{I_j} \phi_m\phi_n \mathrm{d}s,$$
$$M^j_{\rho,nm} = \int_{I_j} \frac{1}{\rho}\phi_m\phi_n \mathrm{d}s,$$

and $\Phi_r = (\phi_1(1),\ldots,\phi_s(1))^T$, $\Phi_l = (\phi_1(-1),\ldots,\phi_s(-1))^T$, $\mathbf{u}^j = (u^j_1,\ldots u^j_s)^{\mathrm{T}}$ and $\mathbf{q}^j = (q^j_1,\ldots q^j_s)^{\mathrm{T}}$. To carry out the numerical implementation, we need to compute matrices M^j, S^j, M^j_ρ, S^j_ρ which are denoted simply as M and S when the same Lengendre basis is used for each subdomain.

Collecting similar terms, we obtain

$$D\mathbf{q}^j + E\mathbf{q}^{j+1} - F\mathbf{q}^{j-1} + \frac{\alpha}{h}(\Phi_r\Phi_r^{\mathrm{T}} + \Phi_l\Phi_l^{\mathrm{T}})\mathbf{u}^j - \frac{\alpha}{h}\Phi_r\Phi_l^{\mathrm{T}}\mathbf{u}^{j+1} - \frac{\alpha}{h}\Phi_l\Phi_r^{\mathrm{T}}\mathbf{u}^{j-1} + M\mathbf{u}^j = \lambda M^j_\rho\mathbf{u}^j, \tag{94}$$
$$\mathbf{q}^j = A\mathbf{u}^j + B\mathbf{u}^{j+1} - C\mathbf{u}^{j-1}, \tag{95}$$

where

$$A = -M^{-1}S + \frac{M^{-1}}{2}(\Phi_r\Phi_r^{\mathrm{T}} - \Phi_l\Phi_l^{\mathrm{T}}), \quad B = \frac{M^{-1}}{2}\Phi_r\Phi_l^{\mathrm{T}},$$
$$C = \frac{M^{-1}}{2}\Phi_l\Phi_r^{\mathrm{T}}, \quad D = -S^j_\rho + \frac{1}{2}\frac{1}{\rho(t_j^+)}(\Phi_r\Phi_r^{\mathrm{T}} - \Phi_l\Phi_l^{\mathrm{T}}),$$
$$E = \frac{1}{2}\frac{1}{\rho(t_{j+1}^+)}\Phi_r\Phi_l^{\mathrm{T}}, \quad F = \frac{1}{2}\frac{1}{\rho(t_j^-)}\Phi_l\Phi_r^{\mathrm{T}}.$$

Now we have

$$G^{j,j-2}\mathbf{u}^{j-2} + G^{j,j-1}\mathbf{u}^{j-1} + G^{j,j}\mathbf{u}^j + G^{j,j-1}\mathbf{u}^{j-1} + G^{j,j+2}\mathbf{u}^{j+2} = \lambda M^j_\rho\mathbf{u}^j, \tag{96}$$

where

$$G^{j,j-2} = FC, \quad G^{j,j-1} = -DC - FA - \frac{\alpha}{h}\Phi_l\Phi_r^{\mathrm{T}},$$
$$G^{j,j} = DA - EC - FB + \frac{\alpha}{h}(\Phi_r\Phi_r^{\mathrm{T}} + \Phi_l\Phi_l^{\mathrm{T}}) + M,$$
$$G^{j,j+1} = DB + EA - \frac{\alpha}{h}\Phi_r\Phi_l^{\mathrm{T}}, \quad G^{j,j+2} = EB.$$

Finally, we obtain the following matrix representation for the eigen-oscillation problem (1) in the discretization of DG approximation

$$G\mathbf{u} = \lambda M_\rho\mathbf{u}, \tag{97}$$

where $\mathbf{u} = (\mathbf{u}^1,\ldots,\mathbf{u}^N)^{\mathrm{T}}$,

$$G = \begin{pmatrix} G^{1,1} & G^{1,2} & G^{1,3} & 0 & 0 & 0 & \ldots & 0 & 0 & 0 \\ G^{2,1} & G^{2,2} & G^{2,3} & G^{2,4} & 0 & 0 & \ldots & 0 & 0 & 0 \\ G^{3,1} & G^{3,2} & G^{3,3} & G^{3,4} & G^{3,5} & 0 & \ldots & 0 & 0 & 0 \\ 0 & G^{4,2} & G^{4,3} & G^{4,4} & G^{4,5} & G^{4,6} & \ldots & 0 & 0 & 0 \\ \ldots & \ldots & \ldots & \ldots & \ldots & \ldots & \ldots & \ldots & \ldots & \ldots \\ 0 & 0 & 0 & 0 & 0 & 0 & \ldots & G^{N,N-2} & G^{N,N-1} & G^{N,N} \end{pmatrix},$$

and (96) will be solved by *eigs* in matlab which calls ARPACK (see [29]).

5.2. Examples of eigenvalues and eigen-oscillations

Let the interval $[0,\pi]$ be discretized uniformly into N subintervals and two different profiles of $\epsilon(x)$ will be considered as follow

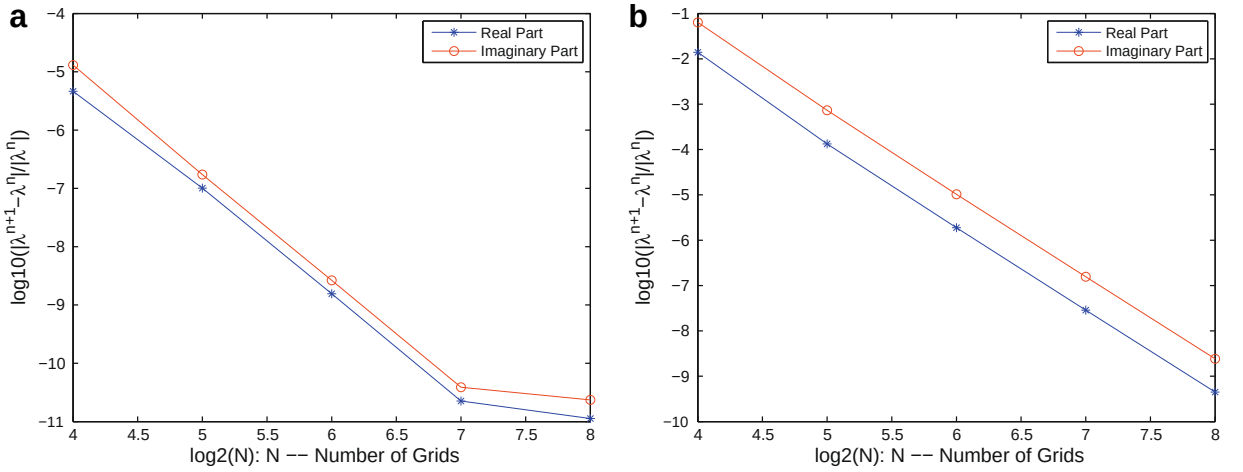

Fig. 3. The convergence of the computed eigenvalues for different mesh points with a discontinuous Galerkin method for $\epsilon = \epsilon_A(x)$. On each subinterval, a 2nd order Legendre polynomial is used. Left: The relative error of the eigenvalue close to $1.479 + 0.1898i$. Right: The relative error of the eigenvalue close to $-21.78 - 0.8667i$.

$$\epsilon_A(x) := \begin{cases} 1 + 0.5i, & x \in [0, \pi/8) \cup \in (7\pi/8, \pi], \\ 2, & x \in [\pi/8, \pi/4] \cup [3\pi/4, 7\pi/8], \\ 3, & x \in [\pi/4, 3\pi/8] \cup [5\pi/8, 3\pi/4], \\ 4, & x \in [3\pi/8, 5\pi/8], \end{cases}$$

and

$$\epsilon_B(x) := \begin{cases} 1 + i, & x \in (0, \pi/2), \\ 2, & x \in (\pi/2, \pi). \end{cases} \tag{98}$$

Hence we have seven layers of dielectric materials in the first case and two layers in the second case. The convergence for certain eigenvalues are shown in Figs. 3 and 4 shows the decrease of the relative error as the number of the grids N increases.

Next, we fix the number of subintervals ($N = 64$) and use different orders of Legendre polynomials as basis functions. The relative error of the eigen-oscillation is calculated as follows. First, we calculated the eigen-oscillation u_n^s corresponding to eigenvalue λ_n using Legendre polynomials of order s. Then we use Legendre polynomials of order $s + 1$ to obtain u_n^{s+1}. The relative error of the eigen-oscillation is given by

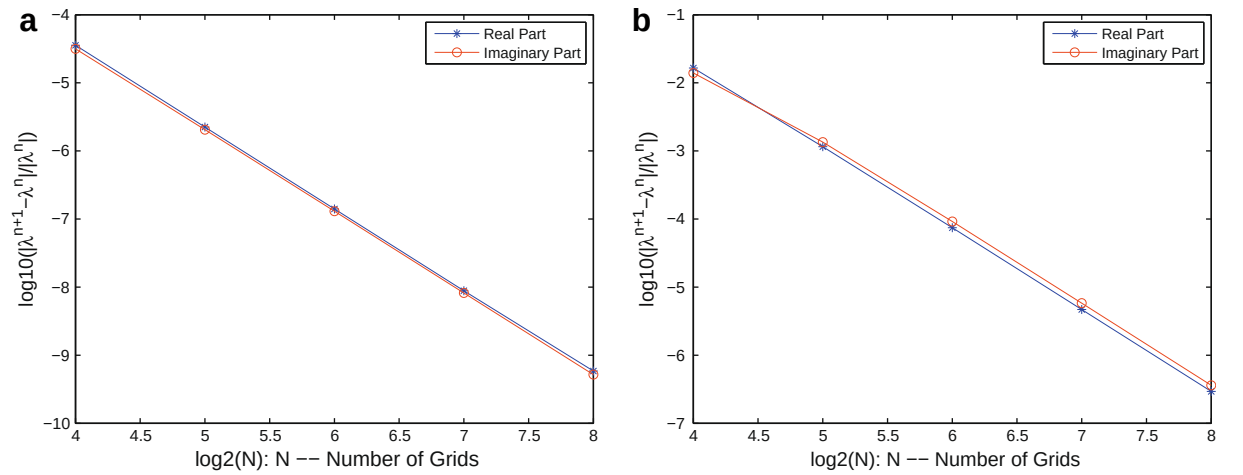

Fig. 4. The convergence of the computed eigenvalues for different mesh points with a discontinuous Galerkin method for $\epsilon = \epsilon_B(x)$. On each subinterval, a 2nd order Legendre polynomial is used. Left: The relative error of the eigenvalue close to $0.5996 + 0.6685i$. Right: The relative error of the eigenvalue close to $-23.40 + 0.7949i$.

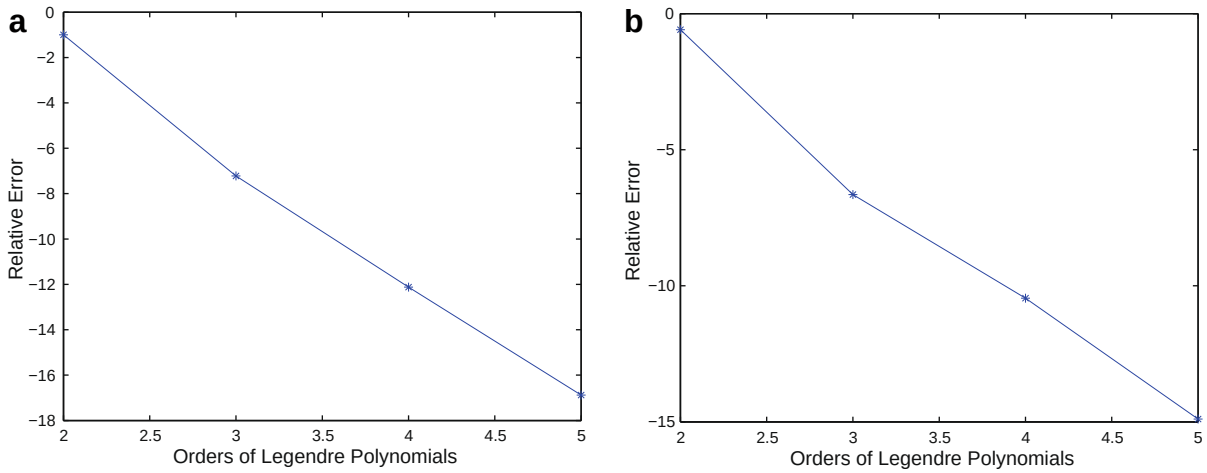

Fig. 5. The relative L_2 error in the eigen-oscillations against the order of polynomials, $\epsilon = \epsilon_B$. Left: the eigen-oscillation for eigenvalue $0.5996 + 0.6685i$. Right: the eigen-oscillation for eigenvalue $-2.591 + 0.2961i$.

$$e^{s+1} = \frac{\|u_n^{s+1} - u_n^s\|_{L^2}}{\|u_n^{s+1}\|_{L^2}},$$

where the L^2 norm is evaluated using Gaussian quadrature. We compute the relative error for $s = 1$ through $s = 4$. Fig. 5 shows the relative L^2 errors against the order of the Legendre polynomials in the calculated eigen-oscillations for two eigenvalues.

6. Numerical results for 2-D complex Helmholtz equations

6.1. PML boundary conditions for scattering waves

The homogeneous Dirichlet boundary conditions in the scattering wave (7) is achieved by terminating the computational domain at the top and bottom with a PML layer [25] as indicated in Fig. 1. In this paper, we apply the formulation of Chew and Weedon [30]. Define a complex-transform coordinate

$$\widetilde{y} = y + \frac{\mathrm{i}}{\sqrt{\omega^2\mu}} \int_a^y \sigma(s)\mathrm{d}s,$$

where a is the starting position of the absorbing layer and σ is some given function. In the absorbing layer, the above coordinate stretching leads to the following equation

$$\left(1 + \frac{\mathrm{i}}{\sqrt{\omega^2\mu}}\sigma(y)\right)\frac{\mathrm{d}}{\mathrm{d}y}\left(\left(1 + \frac{\mathrm{i}}{\sqrt{\omega^2\mu}}\sigma(y)\right)\frac{\mathrm{d}U_{\mathrm{PML}}}{\mathrm{d}y}\right) + \omega^2\mu\epsilon(y)U_{\mathrm{PML}} = 0,$$

or

$$\frac{\mathrm{d}}{\mathrm{d}y}\left(\left(1 + \frac{\mathrm{i}}{\sqrt{\omega^2\mu}}\sigma(y)\right)\frac{\mathrm{d}U_{\mathrm{PML}}}{\mathrm{d}y}\right) + \omega^2\mu\epsilon(y)\left(1 + \frac{\mathrm{i}}{\sqrt{\omega^2\mu}}\sigma(y)\right)^{-1}U_{\mathrm{PML}} = 0.$$

At $y = \pm L$, we apply the homogeneous Dirichlet boundary conditions

$$U_{\mathrm{PML}}(\pm L) = 0. \tag{99}$$

6.2. Layered media

Now we consider the numerical calculation of H_z^s by truncating the series at Nth term in (43), i.e.

$$H_z^s(x,y) \approx \alpha(x)\xi_1(y) + \beta(x)\xi_2(y) + \sum_{p=1}^{N} c_p(x)\phi_p(y). \tag{100}$$

The calculation of A_p and B_p, $p = 1, \ldots, N$ in (33) can be done by using the orthogonality of $\phi_p(y)$ together with suitable boundary conditions. We assume the following Robin type boundary conditions

$$\frac{\partial H_z^s}{\partial x} - ik_x H^s = g_1(y), \quad \text{at } x = 0, \tag{101}$$

$$\frac{\partial H_z^s}{\partial x} + ik_x H^s = g_2(y), \quad \text{at } x = M. \tag{102}$$

Plugging (99) into above equations, multiplying with $\phi_p(y)/\epsilon(y)$ and integrating to obtain, for each p

$$[c_p'(0) + ik_y c_p(0)]d_p + (\alpha'(0) + ik_y\alpha(0))e_p + (\beta'(0) + ik_y\beta(0))f_p = g_{1,p},$$
$$[c_p'(M) + ik_y c_p(M)]d_p + (\alpha'(M) + ik_y\alpha(M))e_p + (\beta'(M) + ik_y\beta(M))f_p = g_{2,p},$$

where

$$d_p = (\phi_p, \phi_p)_\epsilon, \quad e_p = (\xi_1, \phi_p)_\epsilon, \quad f_p = (\xi_2, \phi_p)_\epsilon, \quad g_{1,p} = (g_1, \phi_p)_\epsilon, \quad g_{2,p} = (g_2, \phi_p)_\epsilon,$$

and $(f, g)_\epsilon = \int_{-L}^{L} \frac{1}{\epsilon(y)} f(y)g(y)\mathrm{d}y$. Note that

$$(\phi_p, \phi_q)_\epsilon = 0, \quad p \neq q.$$

Hence we have two equations for A_p and B_p for each $p = 1, \ldots, N$ and they can be solved easily.

For a numerical test, we consider a computation domain $\Omega = [0, \pi] \times [-\pi, \pi]$ and

$$\epsilon(y) := \begin{cases} 1, & y \in [-\pi, 0), \\ 2 + i, & y \in [0, \pi/2), \\ 3, & y \in [\pi/2, \pi]. \end{cases}$$

The incident wave is $H_z^i = \exp(-\mathrm{d}k_x x - \mathrm{d}k_y y)$ such that $k_x^2 + k_y^2 = k^2$. For simplicity, $k_x = 1$ is used in the following computation. To obtain ξ_1, ξ_2 and eigen-oscillations on $[-\pi, \pi]$, we use 64 grid and Legendre polynomials of order 5 in each subinterval. Fig. 6 shows the computed $\xi_1(y)$ and $\xi_2(y)$ for $k = \sqrt{2}$. Note the effects of PML layers on the solutions near two ends of the computational domain.

Let

$$g_1(y) := \begin{cases} 0.1 \times (\pi + y), & y \in [-\pi, 0), \\ 0.1 \times (\pi - y), & y \in [0, \pi], \end{cases}$$

and $g_2(y) = -g_1(y)$. We use 40 eigen-oscillations in (43). For $k = \sqrt{1.01}$, $k = \sqrt{2}$ and $k = \sqrt{101}$, the numerical approximation by the series expansion is shown to have converged. Fig. 7 shows two eigen-oscillations ϕ_4 and ϕ_{15} for $k = \sqrt{2}$. In Fig. 8, we plot $\sqrt{|A_p|^2 + |B_p|^2}$ for different wavenumbers. Fig. 9 shows the computed H_z^s with $k = \sqrt{1.01}$, $k = \sqrt{2}$ and $k = \sqrt{101}$.

6.3. Block media with piecewise constant dielectric constants

Next, we consider the scattering of incident plane waves off a block media with piecewise constant complex dielectric materials, as shown in Fig. 10. The scattering in such a material is of great interest in the design of phase shift mask in the VLSI lithograph technology, where the presence of metal parts in the mask with complex dielectric constants are used to create phase shift of the impinging light rays (within X-ray range for nano-electronics) to induce finer resolution on the chip wafer through wave interference [22]. Non-dimensionalized variables are introduced in these simulations

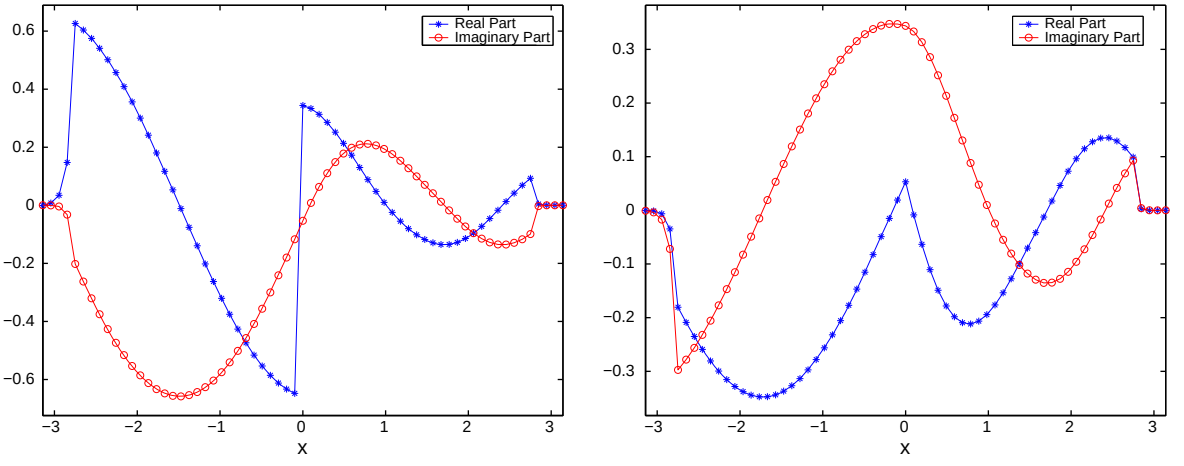

Fig. 6. The real and imaginary part of ξ_1 (left) and ξ_2 (right) for $k = \sqrt{2}$.

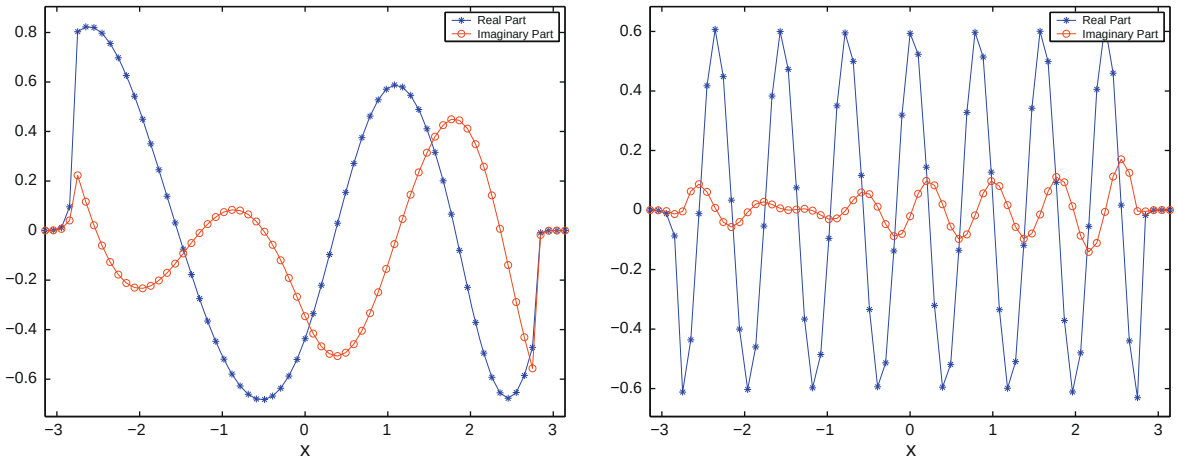

Fig. 7. Two computed eigen-oscillations ϕ_4 and ϕ_{15}.

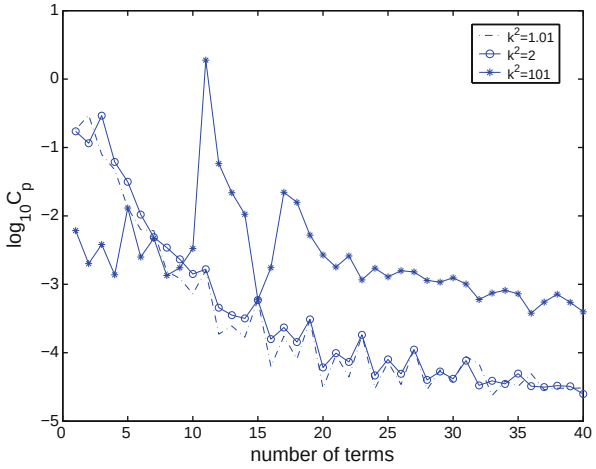

Fig. 8. Decay of the calculated expansion coefficients $\sqrt{|A_p|^2 + |B_p|^2}$ in (33) of GeSEM solutions for different wave numbers.

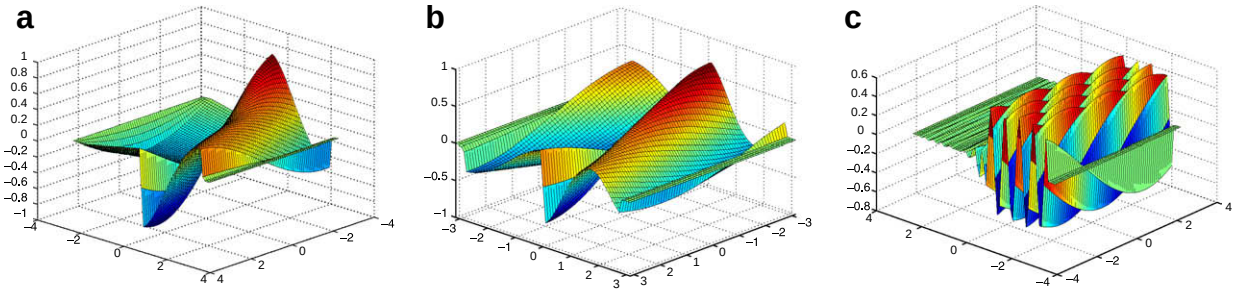

Fig. 9. Computed scattered field H_z^s (real part). Left: $k = \sqrt{1.01}$. Middle: $k = \sqrt{2}$. Right: $k = \sqrt{101}$.

$$\frac{x}{L} \to x, \quad \frac{y}{L} \to y, \quad \frac{ct}{L} \to t, \quad Z_0\mathbf{H} \to \mathbf{H}, \quad \mathbf{E} \to \mathbf{E}, \tag{103}$$

where $L = 1$ rμm is the reference length, c is the speed of light in free space, $Z_0 = \sqrt{\frac{\mu_0}{\epsilon_0}}$ is the free-space impedance. In Fig. 10, one layer of metal grating locates under one layer of dielectric is used in our simulations. The computational domain is $[0,24] \times [0,0.96]$ and the wave number of the incident wave is $k_x = k_y = 10$. The computational domain in the x-direction

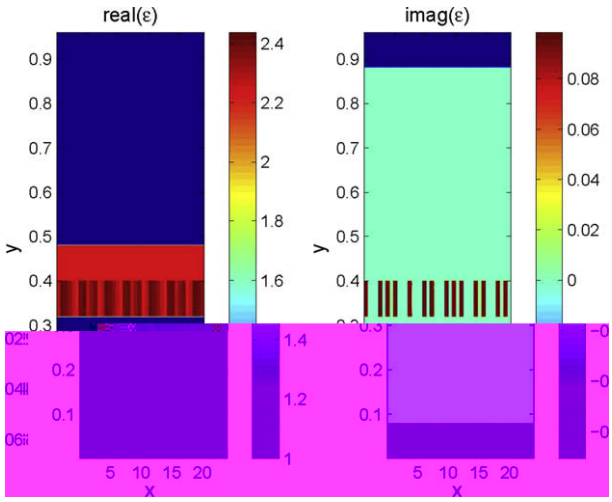

Fig. 10. Distribution of ϵ (piecewise constant case).

is partitioned into 40 subdomains (about one wave length λ in one subdomain) and the y-direction into 12 subdomains with the first and the last subdomain being PML layers. For the Schwarz iteration, the maximum error of the boundary conditions along all vertical interfaces are used as the residual of the Schwarz GeSEM and the error tolerance for convergence is set to be 10^{-6}.

6.3.1. TE wave

Fifteen (15) eigen-oscillations are used along the vertical y direction and eight (8) collocation points are used in the Chebyshev collocation in each subdomain in x-direction. The converged solution obtained by the parallel Schwarz iteration is shown in Fig. 11 where Fig. 11a shows the real part of the total wave and Fig. 11b shows the scattering wave (discontinuity of the field at the top material interface $y = 0.48$ can be observed). The 1-D plot of the H_z field at a fixed $y = 0.3967$ is shown in Fig. 12a. Again, to verify the accuracy of the converged numerical solution, we repeat the GeSEM with a finer mesh (20 eigen-oscillations in y-direction and 10 collocation points for each x-subdomains) and in Fig. 12b, the relative error between these two converged numerical solutions confirms the numerical convergence of the GeSEM method. Fig. 12c shows the convergence of the Schwarz iteration.

6.4. Block media with piecewise linear dielectric constants -TM wave

The advantage of GeSEM in the E_z (TM wave) formulation is that we can handle the case where the dielectric constant is a piecewise linear function of the position. This allows a better approximation to general inhomogeneous media. To test the

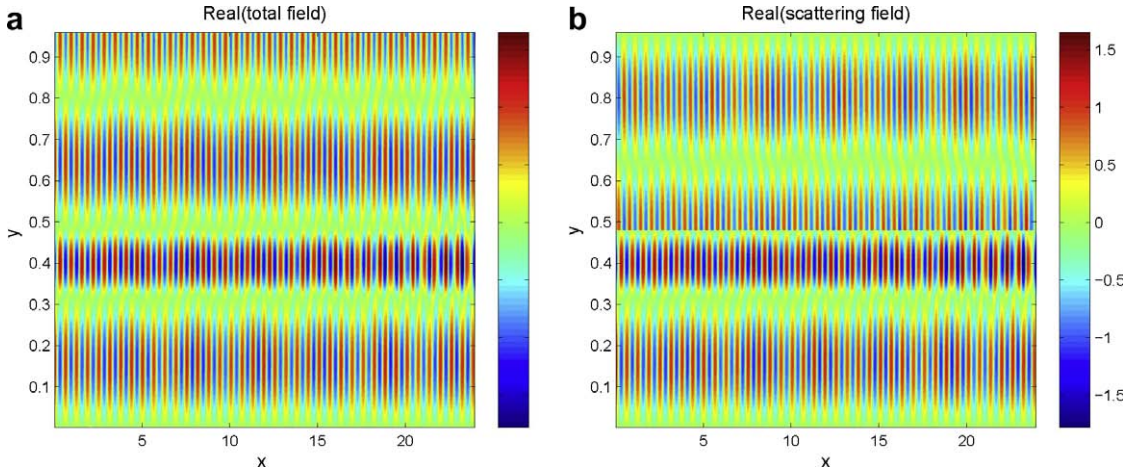

Fig. 11. TE wave: (a) real part of the total wave and (b) real part of the scattering wave.

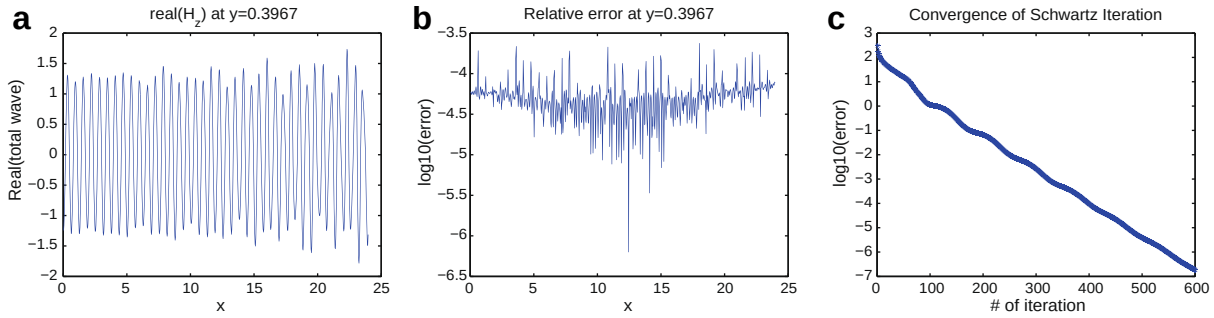

Fig. 12. TE wave: (a) 1-D plot at fixed y, (b) error betwen different basis functions and collocation points, and (c) convergence history of Schwarz iterations.

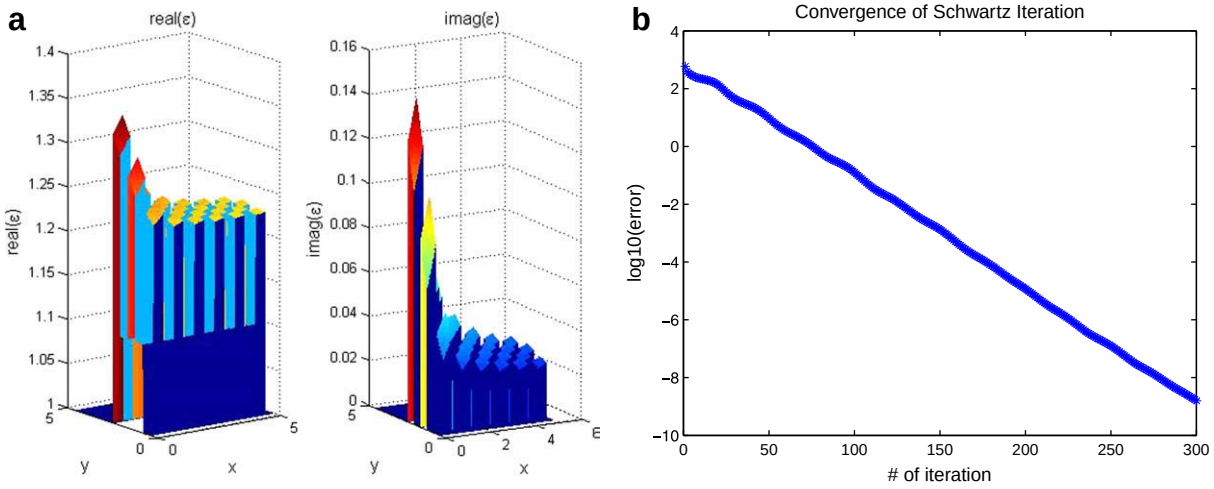

Fig. 13. (a) Distribution of ϵ (linear case). (b) Convergence history of Schwarz iterations (piecewise linear dielectric constant).

GeSEM for this case, we consider a piecewise linear profile of ϵ in Fig. 13a over a domain $[0,5] \times [0,5]$. Again, the wave number of the incidence wave is $k_x = k_y = 10$ and 12 subdomains (about 1.5 wavelength size each) are used in both x and y directions (the first and the last subdomain in y-direction also are PML layers). Fig. 13b shows the convergence of the Schwarz

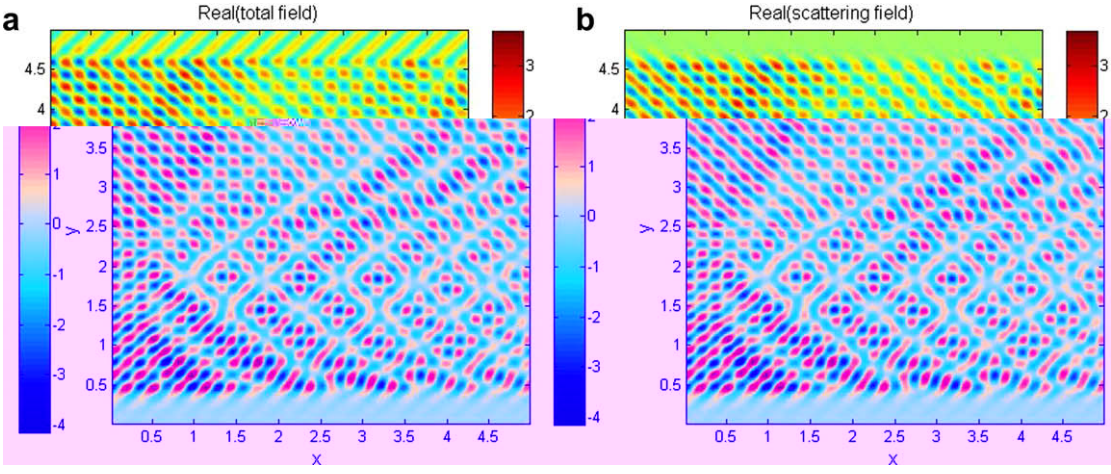

Fig. 14. (a) Real part of the total wave (linear case) and (b) real part of the scattering wave (linear case).

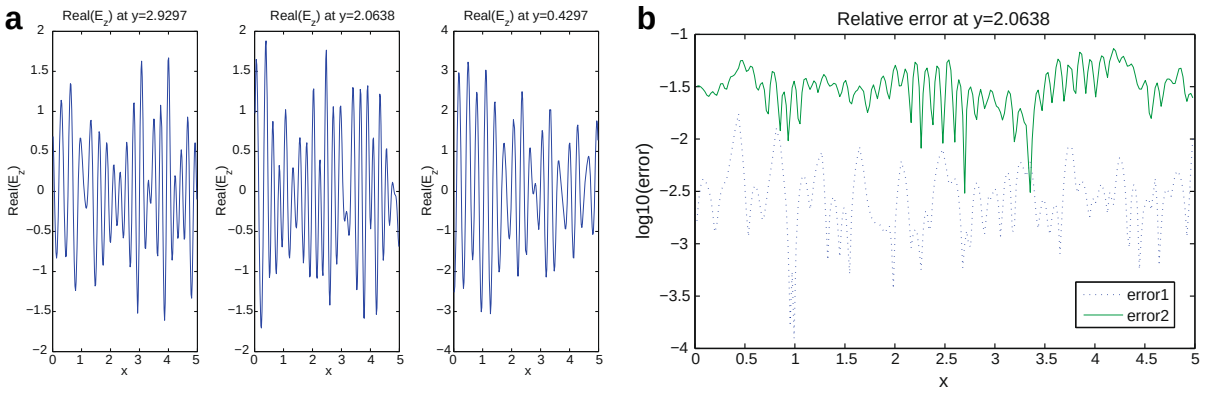

Fig. 15. (a) 1-D plot at fixed y (linear case). (b) Error between different basis functions and collocation points with fixed y (linear case).

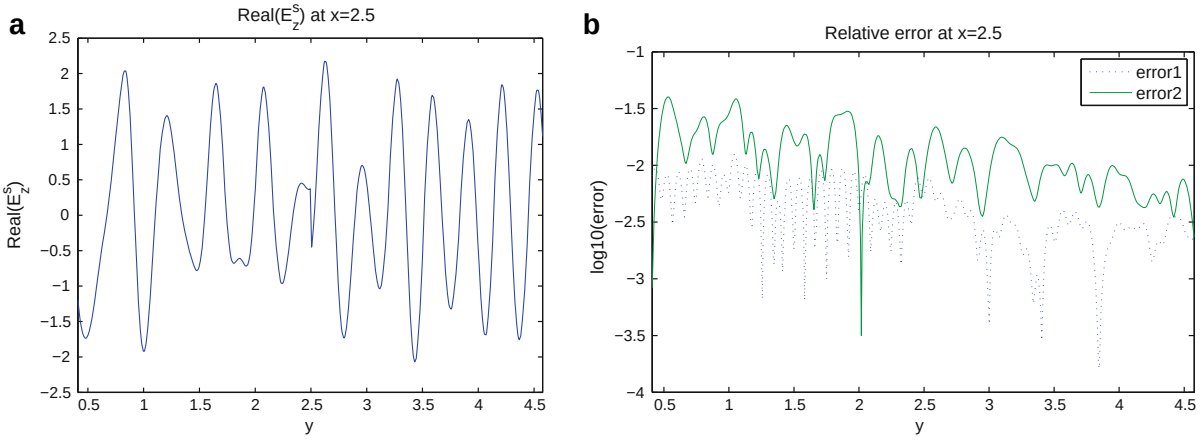

Fig. 16. (a) 1-D plot at fixed x (linear case). (b) Error between different basis functions and collocation points with fixed x (linear case).

iteration. The converged Schwarz GeSEM is given in Fig. 14a – real part of total wave E_z and Fig. 14b – real part of the scattering wave E_z^s. To validate the GeSEM solutions, we compute the solution with three meshes

- Mesh A – 50 eigen-oscillations in y direction and 10 collocation points per subdomain in x direction;
- Mesh B – 55 eigen-oscillations in y direction and 12 collocation points per subdomain in x direction;
- Mesh C – 60 eigen-oscillations in y direction and 14 collocation points per subdomain in x direction.

Fig. 15a is the 1-D plot for E_z field fixing $y = 2.9297, 2.0638, 0.4297$, while Fig. 16a shows the E_z field at a fixed $x = 2.5$. The difference of solutions between Mesh A and Mesh B is identified as error2 and between Mesh B and Mesh C is identified as error1 in Figs. 15b and Fig. 16b, respectively.

7. Conclusions

In this paper, we proposed a parallel generalized eigen-oscillations spectral element method (GeSEM) for complex Helmholtz equations for the scattering of high frequency electromagnetic waves in dispersive inhomogeneous media. The inhomogeneity of the media is approximated by either piecewise constant (TE waves) or piecewise linear (TM waves) dielectric constants. Based on the expansions of complex eigen-oscillations and a non-overlapping Schwarz domain decomposition with a new radiation condition at the domain interfaces, the GeSEM is highly parallel and provides high resolution in the oscillatory fields of high frequency wave interference in inhomogeneous dispersive media. However, many issues remain to be investigated such as the mathematical theory for the extent of validity and convergence of expansions of eigen-oscil-

lations from non-self-adjoint Helmholtz operators and the understanding of the Schwarz iteration with the proposed radiation interface conditions. So far, our numerical results confirmed the convergence of the Schwarz GeSEM when the imaginary part of the dielectric constant is small as indicated by the simple analysis in Appendix. It will be a challenge to resolve the convergence issue for general complex dielectric constants, which will be the topic for further research.

Acknowledgments

The authors thank the support from the Department of Energy (Grant Number: DEFG0205ER25678). Also, they like to thank Profs. Huazhong Tang, Jing Shi and Dr. Zhenli Xu for many interesting discussions during this work and Dr. Kai Fan for improving the presentation of the paper. Sihong Shao is partially supported by China scholarship council (CSC).

Appendix. Convergence of 1-D Schwarz iteration

Here, we present the convergence analysis of Schwarz iteration for Helmholtz equation with piecewise constant coefficients for two subdomains. Denote the interval by $[-a,+a]$ $(a>0)$ and the interface at $x_0 \in (-a,+a)$. The equation under consideration is

$$\left(\frac{1}{\rho(x)}u'(x)\right)' + \sigma^2(x)u(x) = 0, \tag{104}$$

where $\rho(x)$ and $\sigma(x)$ are both piecewise constants, say

$$\rho(x) = \begin{cases} \rho_1, & x \in (-a, x_0) \\ \rho_2, & x \in (x_0, +a) \end{cases}, \sigma(x) = \begin{cases} \sigma_1, & x \in (-a, x_0) \\ \sigma_2, & x \in (x_0, +a) \end{cases}, \tag{105}$$

and the following transmission conditions are imposed:

$$\begin{aligned} &u(x_0^-) = u(x_0^-), \\ &\frac{1}{\rho_1}u'(x_0^-) = \frac{1}{\rho_2}u'(x_0^+). \end{aligned} \tag{106}$$

The Enguist–Majda [10] one way radiation boundary conditions at $\pm a$ are

$$(\partial_x + \mathrm{i}k_1)u(-a) = 0, \quad (\partial_x - \mathrm{i}k_2)u(+a) = 0, \tag{107}$$

where $k_i = \sqrt{\rho_i}\sigma_i$.

As a result, solution $u(x)$ can be written as

$$u(x) = \begin{cases} L\exp(-\mathrm{i}k_1 x) & x \in (-a, x_0), \\ R\exp(+\mathrm{i}k_2 x) & x \in (x_0, +a), \end{cases} \tag{108}$$

where L and R are two undetermined coefficients, which will be computed by the Schwarz iteration. The iteration uses Robin radiation conditions at the interface

$$(\partial_x - \mathrm{i}k_1)u^{n+1}(x_0-) = \left(\frac{\rho_1}{\rho_2}\partial_x - \mathrm{i}k_1 u^n(x_0+)\right), \tag{109}$$

$$(\partial_x + \mathrm{i}k_2)u^{n+1}(x_0+) = \left(\frac{\rho_2}{\rho_1}\partial_x + \mathrm{i}k_2 u^n(x_0-)\right). \tag{110}$$

Using (107), we obtain

$$L^{n+1} = \frac{1}{2}\frac{\rho_1}{\rho_2}(1-z)\exp[\mathrm{i}(k_1+k_2)x_0]R^n, \tag{111}$$

$$R^{n+1} = \frac{1}{2}\frac{\rho_2}{\rho_1}\left(1-\frac{1}{z}\right)\exp[-\mathrm{i}(k_1+k_2)x_0]L^n, \tag{112}$$

where $z = \frac{\rho_2 k_2}{\rho_1 k_1}$.

It follows that

$$L^{n+1} = \frac{1}{4}(1-z)\left(1-\frac{1}{z}\right)L^{n-1}, \tag{113}$$

$$R^{n+1} = \frac{1}{4}(1-z)\left(1-\frac{1}{z}\right)R^{n-1}. \tag{114}$$

Therefore, the convergence rate for the Schwarz iteration using the one-way radiation interface condition (108) and (109) is

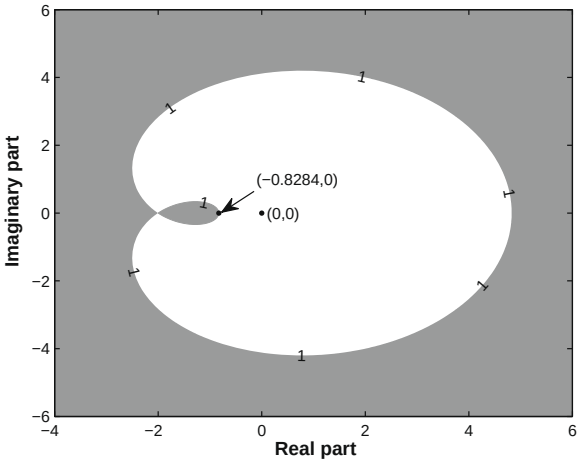

Fig. 17. Region (white) where iteration error reduction factor $\delta < 1$.

$$\delta = \frac{1}{4}(1-z)\left(1-\frac{1}{z}\right).$$

Let $\rho_1 k_1 = \bar{k}$, $\rho_2 k_2 = \bar{k} + \Delta k$, $u = \frac{\Delta k}{k}$, then, $z = 1 + u$, and the convergence rate δ can be rewritten as

$$\delta = \frac{u^2}{4(1+u)}. \tag{115}$$

Fig. 17 shows the domain in the complex u-plane where $|\delta| < 1$ which indicates the size of the variation $\Delta k = \rho_2 k_2 - \rho_1 k_1$ for which the Schwarz iteration converges. It shows that the Schwarz iteration will not converge for dielectric constants with large imaginary parts or with large contrasts or near resonance ($\rho_1 k_1$ or $\rho_2 k_2$ close to zero).

References

[1] D. Colton, R. Kress, Integral Equation Methods in Scattering Theory, Wiley Interscience, New York, 1983.
[2] A. Taflove, S.C. Hagness, Computational Electromagnetics: The Finite-Difference Time-Domain Method, second ed., Artech House, Boston/London, 2000.
[3] J.M. Jin, The Finite Element Method in Electromagnetics, Wiley, New York, 2002.
[4] T. Lu, P.W. Zhang, W. Cai, Discontinuous Galerkin methods for dispersive and lossy Maxwell's equations, J. Comput. Phys. 200 (2004) 549–580.
[5] P.L. Lions, On the Schwarz alternating method III: a variant for nonoverlapping subdomains, in: Proceedings of the Third International Symposium on Domain Decomposition Methods for Partial Differential Equations, SIAM, Philadelphia, PA, 1990, pp. 202–223.
[6] J.D. Benamou, B. Despres, A domain decomposition method for the Helmholtz equation and related optimal control problems, J. Comput. Phys. 136 (1997) 68–82.
[7] X.C. Cai, M.A. Casarin, F.W. Elliott Jr., O.B. Widlund, Overlapping Schwarz algorithms for solving Helmholtz's equation, Domain Decomposition Methods, vol. 10, AMS, Providence, RI, 1998, pp. 391–399.
[8] F. Collino, S. Ghanemi, P. Joly, Domain decomposition method for harmonic wave propagation: a general presentation, Compt. Meth. Appl. Mech. Eng. 184 (2000) 171–211.
[9] M. Gander, F. Magoules, F. Nataf, Optimized Schwarz methods without overlap for the Helmholtz equation, SIAM J. Sci. Compt. 24 (2002) 38–60.
[10] B. Enquist, A. Majda, Absorbing boundary conditions for the numerical simulation of waves, Math. Comp. 31 (1977) 629–651.
[11] D. Gottlieb, S.A. Orszag, Numerical Analysis of Spectral Methods: Theory and Applications, CBMS Conference Series in Applied Mathematics, vol. 26, SIAM, 1977.
[12] C. Canuto, M.Y. Hussaini, A. Quarteroni, T.A. Zang, Spectral Methods in Fluid Dynamics, Springer-Verlag, 1988.
[13] M.S. Agranovich, B.Z. Katsenelenbaum, A.N. Sivov, N.N. Voitovich, Generalized Method of Eigenoscillations in Diffraction Theory, Wiley–VCH, 1999.
[14] R. Hryniv, Y. Mykytyuk, Transformation operators for Sturm–Liouville operators with singular potentials, Math. Phys. Anal. Geometry 7 (2004) 119–149.
[15] X. He, H. Volkmer, Riesz bases of solutions of Sturm–Liouville equations, J. Fourier Anal. Appl. 7 (2001) 297–307.
[16] T. Friese, P. Deuflhard, F. Schmidt, A multigrid method for the complex Helmholtz eigenvalue problem, in: C.H. Lai, P.E. Bjorstad, M. Cross, O.B. Widlund (Eds.), Proceedings of the 11th International Conference on Domain Decomposition Methods in Sciences and Engineering (DD11), UK, 1999, pp. 19–26.
[17] J.S. Hesthaven, T. Warburton, High order nodal discontinuous Galerkin methods for the Maxwell eigenvalue problem, Roy. Soc. London Ser. A 362 (2004) 493–524.
[18] D. Boffi, F. Brezzi, L. Gastaldi, On the problem of spurious eigenvalues in the approximation of linear elliptic problems, Math. Comput. 69 (1999) 121–140.
[19] P.F. Antonietti, A. Buffa, I. Perugia, Discontinuous Galerkin approximation of the Laplace eigenproblem, Comput. Meth. Appl. Mech. Eng. 195 (2006) 3483–3503.
[20] D. Nyyssonen, The theory of optical edge detection and imaging of thick layers, J. Opt. Soc. Am. (1982) 1425.
[21] C.M. Yuan, Calculation of one-dimensional lithographic aerial images using the vector theory, IEEE Trans. Electron Devices (1993) 1604.
[22] H. Tanabe, K.D. Lucas, A.J. Strojwas, Efficient and rigorous three-dimensional model for optical lithography simulation, J. Opt. Soc. Am. (1996) 2187–2199.
[23] K. Zong, X. Ji, X. Zeng, W. Cai, Highly parallel rigorous simulation of phase shift masks with a Generalized Eigen-oscillation Spectral Element Method(GeSEM), IEEE Trans. Electron Devices, preprint, 2008.

[24] C.M. Yuan, Efficient light scattering modeling for alignment, metrology, and rsist exposure in photolithography, IEEE Trans. Electron Devices 39 (7) (1992) 1588.
[25] J.P. Berenger, A perfect matched layer for the absorption of electromagnetics waves, J. Comput. Phys. 114 (1994) 185–200.
[26] A. Zettl, Sturm–Liouville Theory, American Mathematical Society, Providence, Rhode Island, 2005.
[27] Y. Xu, C.W. Shu, Local discontinuous Galerkin methods for nonlinear Schrodinger equations, J. Comput. Phys. 205 (2005) 72–97.
[28] D.N. Arnold, F. Brezzi, B. Cockburn, L.D. Marini, Unified analysis of discontinuous Galerkin methods for elliptic problems, SIAM J. Numer. Anal. 39 (2002) 1749–1779.
[29] R.B. Lehoucq, D.C. Sorensen, C. Yang, ARPACK Users' guide, SIAM, Philadelphia, 1998.
[30] W.C. Chew, W.H. Weedon, A 3D perfectly matched medium from modified Maxwell's equations with stretched coordinates, IEEE Microwave Guided Wave Lett. 7 (1994) 599–604.